PCCP

View Online / Journal Homepage
Dynamic Article Links

Cite this: DOI: 10.1039/c2cp40694b

www.rsc.org/pccp

PAPER

Excited state proton transfer in strongly enhanced GFP (sGFP2)†

Bart van Oort,* Mirelle J. T. ter Veer, Marie Louise Groot and Ivo H. M. van Stokkum*

Received 5th March 2012, Accepted 15th March 2012
DOI: 10.1039/c2cp40694b

Proton transfer is an elementary process in biology. Green fluorescent protein (GFP) has served as an important model system to elucidate the mechanistic details of this reaction, because in GFP proton transfer can be induced by light absorption. We have used pump–dump–probe spectroscopy to study how proton transfer through the 'proton-wire' around the chromophore is affected by a combination of mutations in a modern GFP variety (sGFP2). The results indicate that in H_2O, after absorption of a photon, a proton is transferred (A* → I*) in 5 ps, and back-transferred from a ground state intermediate (I → A) in 0.3 ns, similar to time constants found with GFPuv, although sGFP2 shows less heterogeneous proton transfer. This suggests that the mutations left the proton-transfer largely unchanged, indicating the robustness of the proton-wire. We used pump–dump–probe spectroscopy in combination with target analysis to probe suitability of the sGFP2 fluorophore for super-resolution microscopy.

Introduction

Green Fluorescent Protein (GFP)[1] is an important model system for biologically relevant proton transfer reactions that has been investigated extensively by many spectroscopical methods.[2–10] GFP's excited state proton transfer (ESPT) is unique in biology. The ability to synchronously induce proton transfer with a short laser flash presents a great opportunity to study proton transfer in detail, with high time-resolution. In the past we have studied GFPuv using both visible and IR time-resolved spectroscopy. GFPuv[11] is an "old" variety of GFP. It has surface exposed mutations F99S, M153T and V163A relative to wild-type GFP and is spectrally very similar to the native protein, but 18 times brighter, and it is better soluble in water.[12] In the ground state GFPuv is in a protonated (neutral) form (A). Excitation with 400 nm forms A*, followed by fast intramolecular proton transfer, yielding the deprotonated (negatively charged) chromophore I* that emits green light with a peak at around 510 nm, and a lifetime of ~3 ns in H_2O and a fluorescence quantum yield of 0.79.[13] The intramolecular proton transfer is a multi-exponential process. Four lifetimes were needed to describe the decay of the emission from the A* state, and the longer lifetimes are accompanied by a decreasing probability of forming I*, which approaches zero with the longest A* lifetime of 1.5 ns.[14] Multi-exponentiality also followed from time-resolved difference absorption spectroscopy, where the decay of A* was described by two exponentials of similar amplitude and lifetimes of 2.2 and 11 ps in H_2O, and 12 and 69 ps in D_2O.[15] The multi-exponentiality may be explained by heterogeneity of A and/or by relaxation of A*. The heterogeneity can be linked to the E222 residue which is partially disordered in the ground state.[16,17] Photodecarboxylation of E222 leads to permanent deprotonation of the chromophore (which is then in the anionic form).[17]

The fate of I* has been further studied in GFPuv by pump–dump–probe spectroscopy, which revealed two ground state intermediates (GSIs) I_1 and I_2 after stimulated emission of I*,[15] with lifetimes of 3 ps and 0.4 ns in H_2O, and 7 ps and 5 ns in D_2O. The unusually large kinetic isotope effect suggested the involvement of multiple proton transfer steps, in agreement with results from spectral hole burning.[18] Further studies in D_2O employing also femtosecond IR spectroscopy confirmed the proton transfer and suggested another intermediate between A* and I*, in which a shift of the equilibrium positions of all protons in the H-bonded network has led to a partial protonation of E222 and to a so-called low barrier hydrogen bond (LBHB) for the chromophore's proton, giving rise to dual emission at 475 and 508 nm.[4]

Enhanced GFP (eGFP)[1] was one of the first improved versions of GFP (mutations F64L and S65T, see Fig. S1, ESI†). It showed improved chromophore formation, and the chromophore was deprotonated in the ground state (disrupted proton wire, no ESPT), with a higher extinction coefficient. Other S65T mutants are trapped in state A and show a very broad and asymmetric blue shifted emission spectrum, with an excited state decay time of only a few hundred picoseconds. This is in sharp contrast to the narrow slightly structured emission of I* which is associated with a fluorescence lifetime of a few nanoseconds.[19] Strongly enhanced

Institute for Lasers, Life and Biophotonics, Faculty of Sciences, VU University Amsterdam, De Boelelaan 1081, 1081 HV Amsterdam, The Netherlands. E-mail: b.f.van.oort@vu.nl, i.h.m.van.stokkum@vu.nl; Fax: +31 205987992; Tel: +31 205987868

† Electronic supplementary information (ESI) available: (1) Photo-conversion in sGFP2. (2) Comparison of kinetics of sGFP2 and GFPuv. (3) Model based data analysis. See DOI: 10.1039/c2cp40694b

GFP (sGFP2) is a more recent improvement of eGFP, with five additional mutations (S72A, M153T, V163A, S175G and A206K),[20] leading to improved protein folding and solubility and decreased tendency to dimerize. sGFP2 has similar brightness to eGFP, despite partial protonation in the ground state. sGFP2 variants without protonation had low quantum yields (T65G) or slow folding (E222Q).

Here we choose to study the ESPT in sGFP2, because it is a modern type of GFP, which is more relevant for microscopy than GFPuv, and because in contrast to most other eGFP variants it shows (partial) protonation in the ground state which makes it an interesting system to study ESPT. In particular it is interesting to study how the proton transfer is affected by the additional mutations. Furthermore this study presents a way to screen for suitable GFP variants for super-resolution microscopy. The role therein of GFP's ground state intermediates is discussed.

Materials and methods

His_6-tagged strongly enhanced GFP (sGFP2) was prepared as described previously.[20] In brief, sGFP2 was expressed in *Escherichia coli* for 5 h at room temperature, and purified using His-bind Resin (Novagen, Darmstadt, Germany). It was frozen in liquid nitrogen and stored at −80 °C until usage. Samples were measured in 20 mM Tris buffer (pH = 8) in 1 mm path length quartz cuvettes, at an OD of 0.25–0.35 mm^{-1} at 400 nm. Oxygen was removed with an oxygen scavenging system of glucose oxidase, catalase and glucose. Sample quality was checked by steady state absorption (Lambda40 photospectrometer, Perkin-Elmer, Wellesley, MA, USA) before and after PDP experiments, which showed for some experimental signs of photoconversion (see ESI†). All experiments were performed at room temperature.

Multi-pulse visible pump–dump–probe measurements were performed on the set-up described previously, based on a set of commercial lasers and amplifiers (Coherent Inc., Santa Clara, CA, USA).[4,21] In brief, a 1 kHz Ti:sapphire oscillator and amplifier provided <100 fs 800 nm pulses, which were split into three paths. The first path was frequency doubled in a BBO crystal to give the 400 nm pump pulses. The second path was used to pump an Optical Parametric Amplifier, producing dump pulses at 550 and 575 nm, and the third path was focused into a rotating CaF_2 plate generating broadband probe pulses, ranging from 430 nm to 750 nm. The transient absorption of the probe pulse was measured by dispersing the probe beam in an imaging spectrograph (Newport Oriel MS127i) with a photodiode array (Hamamatsu S3901-256Q). The delay time between pump and dump pulses was 1, 5, 10 or 50 ps. This delay time was varied synchronously relative to the delay time of the probe pulses, using two automated translation stages of 60 cm. Pump pulses were modulated with a chopper at 500 Hz, and the dump pulses at 250 Hz, while detecting at 1 kHz. This generated 4 datasets, in the presence of one, two or three laser pulses: pump–dump–probe, pump–probe, dump–probe and probe-only (control). Polarization of pump and dump pulses was set parallel to each other at a magic angle relative to that of the probe pulse. Pump pulse energy was set at 170 nJ, and dump pulse energies varied between 200 nJ and 600 nJ. The temporal instrument response function was ~0.42 ps full width at half maximum and the spectral resolution was ~1 nm. The data were fitted by using global and target analysis,[22] with the extension for pump–dump–probe data described in ref. 15. Model based data-analysis is described in more detail in the ESI.† The absorption and emission spectra of sGFP2 are shown in Fig. 1, together with the profiles of the laser pulses.

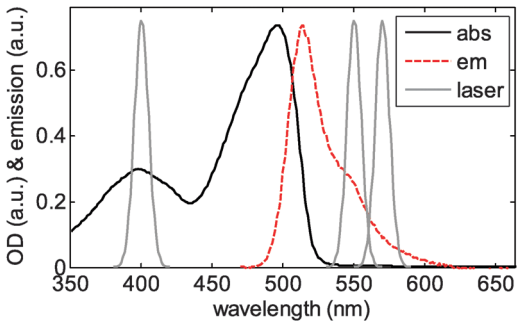

Fig. 1 Steady state absorption (black) and emission (red dashed) spectra of sGFP2 and spectra (grey) of the 400 nm pump and 550 and 575 nm dump laser pulses.

Results and discussion

Pump–probe (PP) spectroscopy

A typical PP dataset of sGFP2 excited at 400 nm is shown in Fig. 2a, with transient spectra and time-traces in Fig. 2d and e. The PP signal consists of a positive band at around 450 nm (excited state absorption, ESA) and a negative band at around 520 nm. This band consists of ground state bleach (GSB), stimulated emission (SE) and perhaps a minor contribution of the broad weak ESA-band that extends to over 700 nm. The band rapidly red-shifts and rises within several picoseconds. The GSB of the 400 nm absorption band is not within the detection range.

The data were fitted with a three-component sequential scheme (Fig. 2f–h). In this model the 400 nm pulse excites molecules from the ground state to an initial excited state, with absorption difference spectrum SADS1 (SADS = species associated decay spectrum, see ESI†). SADS1 (black in (g)) shows a positive ESA band at 450 nm and a broad negative band peaking at 520 nm. This spectrum is very similar to that observed in GFPuv,[15] where the chromophore is protonated in the ground state. Therefore we attributed SADS1 to the protonated excited state A*. Apparently 400 nm light excites almost exclusively the subpopulation of sGFP2 proteins with protonated chromophores (this was confirmed by allowing direct excitation of SADS2 in the fit, yielding $\leq 3\%$ of SADS2 excitation). In 5 ps SADS1 evolves to SADS2, with stronger ESA at 450 nm and increased, narrowed and red-shifted stimulated emission. In GFPuv this spectrum is assigned to the deprotonated chromophore, I*.[15] In 2.8 ns SADS2 evolves to SADS3, which shows no stimulated emission, indicating that it is an electronic ground state intermediate (GSI) rather than an excited state. The transient concentration of SADS3 is very small (Fig. 2h), due to the inverted kinetics (slow rise (k_2), rapid

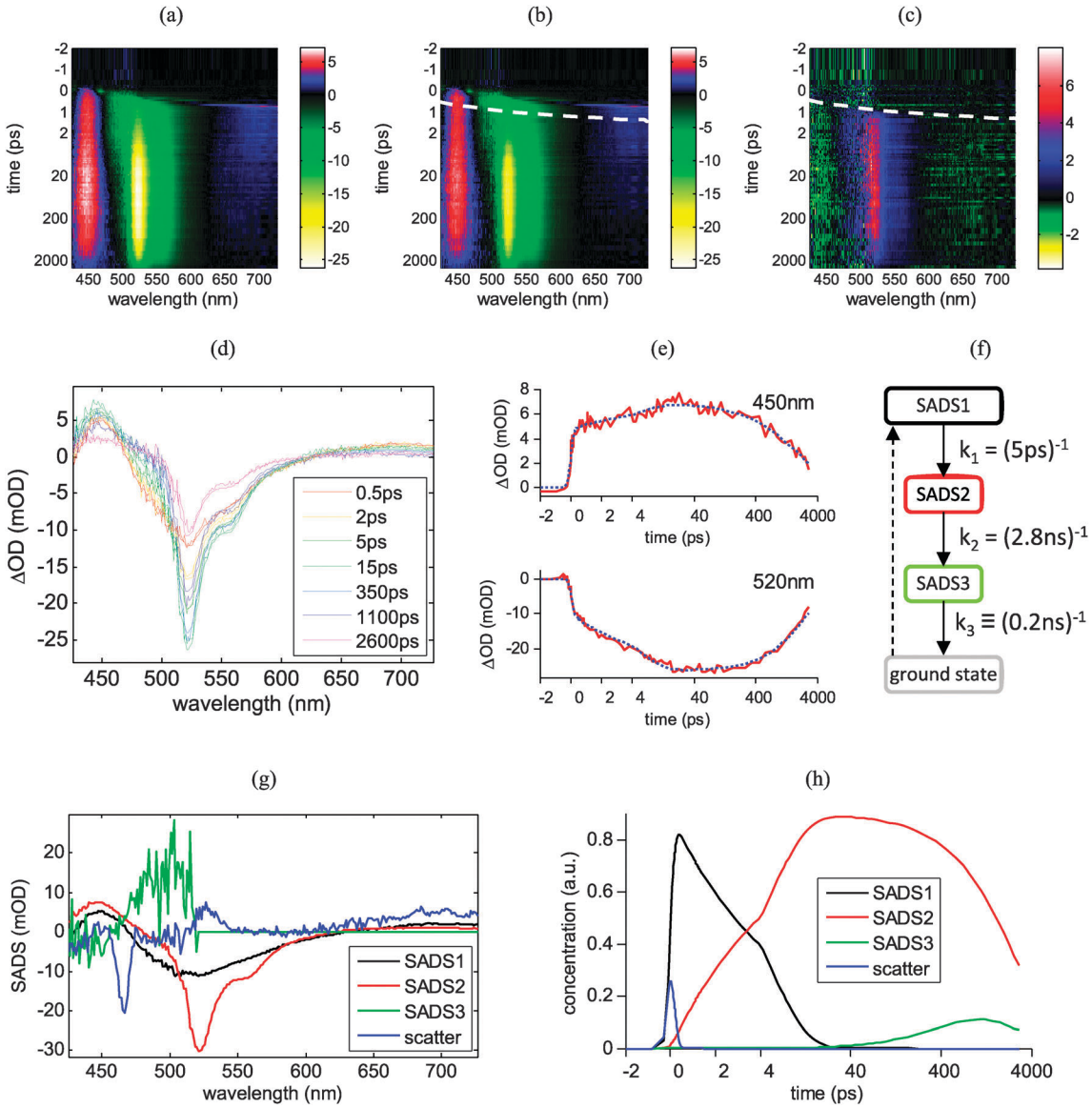

Fig. 2 Pump–dump–probe data and fit of PP of sGFP2 excited at 400 nm. (a) Color coded PP data in mOD. The time-axis is linear until 2 ps, and logarithmic thereafter, (b) same for PDP–DP, and (c) PDP–DP–PP; the white dashed line indicates the dumping time. (d) Selected PP transient spectra and fits (dotted), (e) selected PP time traces and fits (dotted) at 450 nm (upper) and 520 nm, (f) PP fit model with fitted rates (k_3 was fixed), (g) species associated difference spectra (SADS; SADS3 scaled by 0.5 for visibility) and (h) concentration time-profiles from the fit. The transient spectra in (d) at $\leq$5 ps were corrected for dispersion. The time-axis in (e) and (h) is linear until 4 ps, and logarithmic thereafter. The blue traces in (g) and (h) are attributed to scattered and coherent artifact.

decay (k_3)). Therefore it is hard to characterize. In particular, the lifetime and spectral amplitude cannot be estimated independently, so k_3 had to be fixed for the fit to converge. Higher transient concentrations of GSI are obtained by extension of the experiment with a dump pulse, which forcibly populates the GSI *via* stimulated emission (*vide infra*).

In summary, the pump–probe experiments show the presence of an initial protonated excited state (A*), which rapidly evolves into a deprotonated state (I*), which decays on a nanosecond timescale to a protonated ground state intermediate (GSI), followed by proton back-transfer on the timescale of hundreds of picoseconds. The difference absorption spectra and kinetics are similar to those in GFPuv, indicating that the sequential (evolutionary) scheme describes true physical states. More detailed characterization of the GSI requires pump–dump–probe spectroscopy.

Pump–dump–probe (PDP) spectroscopy

In pump–dump–probe spectroscopy three short laser pulses are employed. The first (pump) pulse creates excitations, which are allowed to evolve during time t_{dump} (dump time), after which the second pulse (dump) interacts with the sample, inducing dumping (*via* stimulated emission) and/or repumping (*via* excited state absorption). After time Δt (with $t_{probe} = \Delta t + t_{dump}$, and t_{probe} the probe time) the transient absorption spectrum is recorded with the third (probe) pulse. The transient spectra in the presence of either pump, dump or both

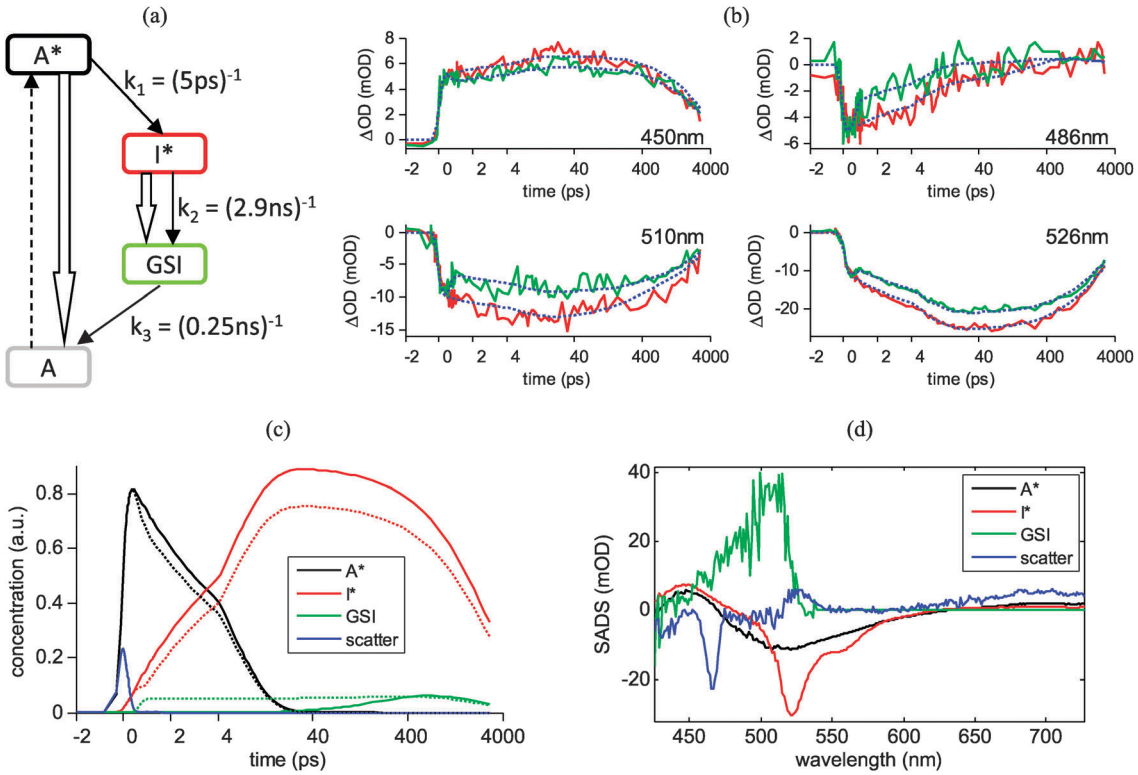

Fig. 3 Results of simultaneous target analysis of the data in Fig. 2a and b. (a) target model, (b) selected time traces and fits (dotted blue line) (red and green lines indicate PP and PDP–DP respectively), (c) concentration time-profiles (solid and dotted lines indicate PP and PDP–DP respectively), (d) species-associated difference spectra. The time-axes are linear until 4 ps, and logarithmic thereafter. For better visibility, the green spectrum in (d) is multiplied by 0.5, and the green concentration in (c) is multiplied by 2. The blue traces in (c) and (d) are instantaneously scattered light and coherent artefact. In (a) the dashed arrow indicates excitation by the 400 nm pulse, the block-arrows dumping by the 575 nm pulse and the regular arrows spontaneous processes.

pulses are measured for variable t_{probe} and fixed t_{dump}, yielding datasets named, respectively, PP, DP and PDP. PDP spectroscopy is ideally suited to create high transient concentrations of states that are otherwise only slightly populated. This is the case with the GSI in Fig. 2.

For sGFP2, a dump pulse of 575 nm was applied at t_{dump} = 1 ps after the pump pulse (Fig. 2b; DP data were subtracted from PDP to correct for the coherent artefact and a small amount (0–4%) of excitation by the dump pulse). Dumping is clearly visible as a loss of signal after 1 ps (compare Fig. 2a). The product formed by dumping is observed more clearly as (PDP–DP)–PP (Fig. 2c), and shows a positive band at 510 nm, and weak bleach at $<$440 nm. This product decays on a time scale of hundreds of picoseconds.

The PDP–DP data were fitted simultaneously with the PP dataset, using the target model shown in Fig. 3a (see ESI† for details on the global and target analysis). In this model the 400 nm pump pulse excites only sGFP2 proteins in the protonated state (A), yielding the protonated excited state A*, which subsequently converts to the (deprotonated) excited state I* in 5 ps. In 2.9 ns I* decays to the (deprotonated) ground state I, a ground-state intermediate (GSI), which reverts to A in 0.25 ns. The 575 nm dump pulse (block-arrows in Fig. 3a) de-excites A* to A (ground state), which has no absorption difference spectrum, and I* to GSI. De-excitation of A* reduces the amount of I* formation, and therefore also the amount of GSI formed on the nanosecond scale. De-excitation of I* leads to an instantaneous drop in the concentration of I* equal to the rise in the concentration of GSI.

The model in Fig. 3a is by no means the only model that can describe the PDP data. Therefore several alternative models were tested. First, inclusion of direct excitation of I to I*. This resulted in only a small fraction of direct excitation (a few percent relative to A*), which varies between experiments. Fitted lifetimes and spectra were not affected, and the fit quality improved only very little. Second, inclusion of bi-exponential conversion of A* to I* and of GSI to A. This resulted in A* $\rightarrow$ I* rates varying strongly between experiments, indicating that at the current signal-to-noise bi-exponentiality is not detectable (this is studied in more detail in the ESI†). Third, inclusion of dumping of A* to the GSI. This resulted in a decreased amplitude of the GSI spectrum, and was no longer consistent with dumping at later dump times when the concentration of A* is much smaller than I* (*vide infra*).

Thus, the model in Fig. 3 is the simplest to satisfactorily describe the data. The species associated absorption difference spectra (SADS) of A* and I* of this simultaneous fit are very similar to those from the fit of only the pump–probe data (Fig. 2), confirming the assignment of those difference spectra. It is concluded that A* is dumped to the ground state (A), whereas I* is dumped to a GSI. Quantitatively, after unit excitation 0.085 A* and 0.034 I* are dumped at a 0.8 ps delay

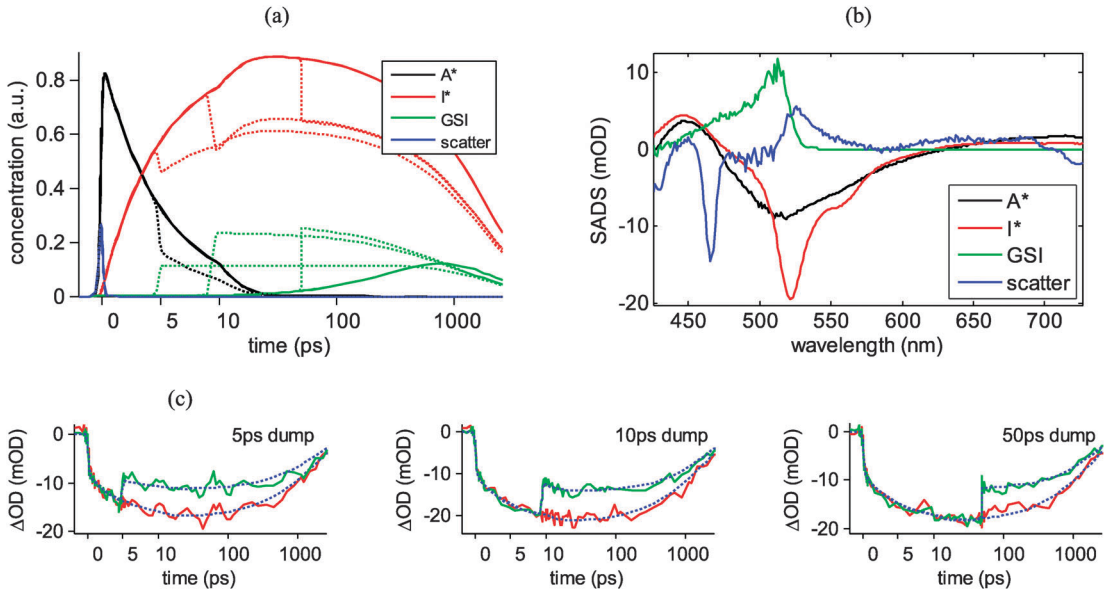

Fig. 4 Results of simultaneous fitting of the datasets with 575 nm dumping at delay times of 5, 10 and 50 ps with the model in Fig. 3a. (a) Concentration time-profiles, (b) species-associated difference spectra and (c) time traces and fits (dotted blue lines) of PP (red) and PDP-DP (green) at 520 nm, dumped at 5 ps (left), 10 ps (middle) and 50 ps (right). The time-axes are linear until 10 ps, and logarithmic thereafter. The blue traces in (a) and (b) are instantaneously scattered light and coherent artefact. The different amounts of dumping at different dump times are due to different dump powers and A* and I* concentrations.

time. Since GSI is formed only from I*, the experiments were extended with dumping at longer delay times, when the higher I* concentration should yield more GSI.

PDP experiments with 575 nm dumping at 5, 10 and 50 ps were fitted simultaneously (Fig. 4) with the model in Fig. 3a, assuming equal spectra and transfer rates for all experiments. The decay rate of I* showed some variability in the fits of individual datasets, so it was allowed to differ between experiments, yielding values ranging from $k_2 = (1.9\ \text{ns})^{-1}$ to $(2.8\ \text{ns})^{-1}$, in good agreement with previously reported values from time-resolved microscopy.[23,24] Experiments of partly photoconverted sGFP2 showed shorter I* lifetimes than unconverted proteins (see ESI†), providing a possible explanation for the variability of I* lifetime. The rate of A* → I*, $k_1 = (4.8 \pm 0.4\ \text{ps})^{-1}$, was identical to the 1 ps PDP fit. The rate of GSI → A, $k_3 = (0.38\ \text{ns})^{-1}$, was somewhat slower than in the fit above. Alternative fit models were tested, as described above, with similar results. In addition, a variable amplitude of the GSI spectrum among the different datasets was tested, which had no effect on the rates and spectra. Based on the results of all these fits we conclude that $k_3 = (0.3 \pm 0.1\ \text{ns})^{-1}$. The GSI spectrum can be estimated much more accurately from this fit than before (compare the noise levels of the green spectra in Fig. 4b, 3d and 2g).

The target model was tested by PDP experiments with dumping at 550 nm (Fig. 5), where the stimulated emission amplitudes of I* and A* are different from those at 575 nm (the SADS at these wavelengths consists mainly of stimulated emission, as deduced from PP experiments of GFP(S65T)).[25] Dumping at 550 nm gives the same GSI as dumping at 575 nm (compare Fig. 4 and 5), but with stronger dumping efficiency. Relatively more I* is dumped than A*, in agreement with their stimulated emission amplitudes. More GSI is formed with 550 nm dumping, confirming that the GSI is formed from

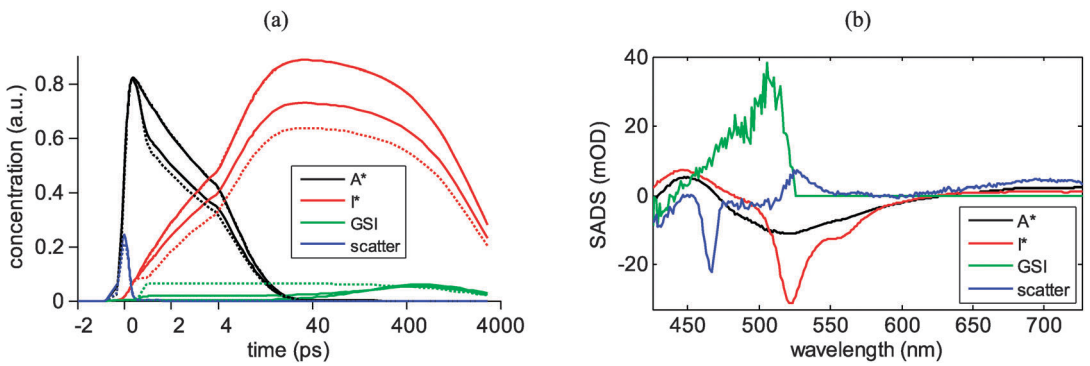

Fig. 5 Results of the simultaneous fit of the datasets with 550 nm (dotted) and 575 nm dumping at 1 ps with the model in Fig. 3a. (a) Concentration time-profiles and (b) species-associated difference spectra. In the absence of dumping the time-traces overlap. The time-axis in (a) is linear until 4 ps, and logarithmic thereafter.

I* but not from A*. Thus these experiments confirm the target model. Moreover, they prove that it is possible to selectively dump A* or I* by careful selection of the dumping wavelength. In the case of A* dumping no ground state intermediate is formed. This may be relevant for suitability of sGFP2 for super-resolution microscopy.

Application to super-resolution microscopy?

At 400 nm exclusively the protonated (A) state of sGFP2 is excited (Fig. 2), followed by excited state proton transfer (ESPT) forming I* which decays to the A state *via* a ground state intermediate (GSI). This is similar to the kinetics of GFPuv,[15] except for two aspects: firstly, the A* → I* transition is slightly faster in sGFP2, and showed no signs of bi-exponential behavior, indicating that excited state proton transfer may be less heterogeneous in sGFP2 than in GFPuv. In Fig. S3 (ESI†) we compare traces from sGFP2 and GFPuv at the minimum of the I* SADS, and demonstrate the difference in the rise of I*. Secondly, the GSI → A transition lacks the fast blue-shift (3 ps) from a primary (I_1) to a secondary (I_2) GSI of GFPuv.[15] The SADS of GSI in sGFP2 nicely mirrors the emission spectrum (green and red lines in Fig. 6), as evidenced by the narrow peak (half maxima at approximately 495 and 525 nm) and shoulder near 475 nm. The energy difference between the 0–0 transitions GSI ↔ I* is so small that, unlike in GFPuv, in sGFP2 ground-state proton back-transfer is a mono-exponential process.

Apparently, in the sub-population of sGFP2 proteins with protonated chromophores, the proton-transfer-wire is slightly different from that in GFPuv. The mono-exponential A* → I* transition in sGFP2 points to minor changes in the proton-network in the excited state, or possibly less disorder of the E222 residue in the ground state of the protonated sGFP2 mutant.[16] This could also explain the homogeneous proton back-transfer. Interestingly, though the major fraction of the sGFP2 proteins has its chromophore in the deprotonated state, creation of the deprotonated chromophore in its ground state with light results in an efficient reformation of the protonated chromophore with a 0.3 ns time constant. This shows that the protein environment that determines whether the energetically favourable state contains a protonated or deprotonated chromophore is stable on the time scale from 0.1 ps to 3 ns. The huge difference between the timescales of proton transfer in the excited state A* → I* and in the ground state GSI → A, 5 ps *vs.* 0.3 ns, can be explained by an increased energy barrier for the GSI → A transition, as in GFPuv and wtGFP.[4,15,18] It would imply that proton back-transfer is thermally activated, and that the GSI plays an important role in sGFP2's photocycle. Further experiments with time resolved IR spectroscopy will be needed to further unravel the dynamics in the hydrogen bonding network.[4,26]

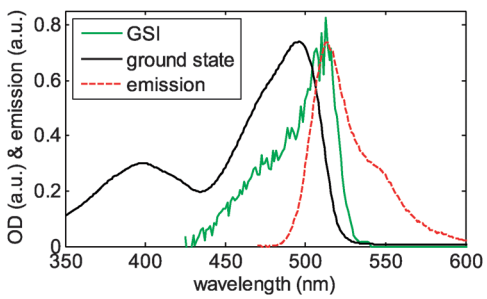

Fig. 6 Steady state absorption and emission spectra of sGFP2 (black and red dashed line), and ΔOD of GSI from Fig. 4b (green).

Ground state and excited state processes determine the suitability of fluorescent proteins for optical microscopy, and in particular super-resolution microscopy, *e.g.* stimulated emission depletion (STED) microscopy.[27] STED is a very powerful technique in life sciences,[28] based on local de-excitation of excited chromophores *via* stimulated emission. However, experiments with fluorescent proteins (*e.g.* ref. 25, 29–31) usually yield lower resolution results than with organic dyes (*e.g.* ref. 32 and 33). This is mainly due to the lower brightness and stronger photobleaching of fluorescent proteins, which often occurs *via* excited state absorption. It is therefore crucial to select the right "STED-wavelength", where the stimulated emission cross-section is high, while the excited state absorption is low. Pump–probe spectroscopy has been successfully applied to find suitable wavelengths for eGFP (supporting material in ref. 25) and two organic dyes.[32] It is also crucial to select the right fluorophores. One of the determining factors therein is the presence of long-lived (initial) GSI's, which limit dumping efficiency, due to the Frank–Condon principle. Consequently the power and/or duration of the STED beam has to be raised, leading to additional photobleaching. Moreover, photon absorption by GSI's may lead to additional photobleaching. PDP spectroscopy is a rarely used, but very useful method to study the presence and lifetime of GSI's. For sGFP2 we found a long-lived GSI, rendering the protein ill-suited for STED. However, the possibility to selectively de-excite A* at a specific wavelength enables by-passing of the GSI, and may offer a solution. The required wavelength was chosen from the SADS's and tested by PDP (see Fig. 5). Without PDP experiments it would have been impossible to test for GSI formation from A*. GFPuv may be more suited for STED than sGFP2, due to the presence of the short-lived GSI I_2.[15] Both sGFP2 and GFPuv offer the advantage of a large difference between excitation (~400 nm) and de-excitation (~550 nm) wavelengths, leaving a large spectral window for fluorescence detection.

In conclusion, PDP spectroscopy offers the following tools to support fluorescence microscopy: (1) unique information on ground state processes, which are important for fluorophore selection; and (2) PP data, which provide the ESA and SE spectra that are important for wavelength selection.

Conclusions

We demonstrated that

(i) after A* → I* excited state proton transfer (ESPT, rate $(5\ ps)^{-1}$) sGFP2 has a ground-state intermediate, related to thermally activated proton back-transfer GSI → A. The rate of this back-transfer is $(0.3 \pm 0.1\ ns)^{-1}$ in H_2O.

(ii) sGFP2 is only the second fluorescent protein for which a GSI has been shown to exist. GSI's are important elements of the photocycle of GFP and related proteins, and as such important for a full understanding of the protein dynamics.

(iii) proton transfer in sGFP2 is more homogeneous (mono-exponential), but is overall similar to that in GFPuv,

suggesting that despite the large changes in the amino acid sequence, the proton network around the chromophore is not much affected.

(iv) PDP spectroscopy in combination with target analysis is a useful tool to probe suitability of a fluorophore for STED microscopy.

Acknowledgements

We thank Linda Joosen (van Leeuwenhoek Centre of Advanced Microscopy, Amsterdam) for kindly providing the sGFP2 sample. John Kennis is thanked for critical reading of the manuscript. BvO acknowledges the Dutch Ministry of ELI through the BioSolar Cells Project for financial support, and the Netherlands Organisation for Scientific Research (NWO) for a Rubicon Grant.

Notes and references

1 R. Y. Tsien, *Annu. Rev. Biochem.*, 1998, **67**, 509–544.
2 S. R. Meech, *Chem. Soc. Rev.*, 2009, **38**, 2922–2934.
3 P. J. Tonge and S. R. Meech, *J. Photochem. Photobiol., A*, 2009, **205**, 1–11.
4 M. Di Donato, L. J. G. W. van Wilderen, I. H. M. Van Stokkum, T. C. Stuart, J. T. M. Kennis, K. J. Hellingwerf, R. van Grondelle and M. L. Groot, *Phys. Chem. Chem. Phys.*, 2011, **13**, 16295–16305.
5 M. Chattoraj, B. A. King, G. U. Bublitz and S. G. Boxer, *Proc. Natl. Acad. Sci. U. S. A.*, 1996, **93**, 8362–8367.
6 H. Lossau, A. Kummer, R. Heinecke, F. PollingerDammer, C. Kompa, G. Bieser, T. Jonsson, C. M. Silva, M. M. Yang, D. C. Youvan and M. E. MichelBeyerle, *Chem. Phys.*, 1996, **213**, 1–16.
7 D. Stoner-Ma, A. A. Jaye, P. Matousek, M. Towrie, S. R. Meech and P. J. Tonge, *J. Am. Chem. Soc.*, 2005, **127**, 2864–2865.
8 D. Stoner-Ma, A. A. Jaye, K. L. Ronayne, J. Nappa, S. R. Meech and P. J. Tonge, *J. Am. Chem. Soc.*, 2008, **130**, 1227–1235.
9 G. Striker, V. Subramaniam, C. A. M. Seidel and A. Volkmer, *J. Phys. Chem. B*, 1999, **103**, 8612–8617.
10 K. Winkler, J. R. Lindner, V. Subramaniam, T. M. Jovin and P. Vohringer, *Phys. Chem. Chem. Phys.*, 2002, **4**, 1072–1081.
11 J. J. van Thor, A. J. Pierik, I. Nugteren-Roodzant, A. H. Xie and K. J. Hellingwerf, *Biochemistry*, 1998, **37**, 16915–16921.
12 G. H. Patterson, S. M. Knobel, W. D. Sharif, S. R. Kain and D. W. Piston, *Biophys. J.*, 1997, **73**, 2782–2790.
13 S. Topell, J. Hennecke and R. Glockshuber, *FEBS Lett.*, 1999, **457**, 283–289.
14 I. H. M. van Stokkum, B. Gobets, T. Gensch, F. van Mourik, K. J. Hellingwerf, R. van Grondelle and J. T. M. Kennis, *Photochem. Photobiol.*, 2006, **82**, 380–388.
15 J. T. M. Kennis, D. S. Larsen, I. H. M. van Stokkum, M. Vengris, J. J. van Thor and R. van Grondelle, *Proc. Natl. Acad. Sci. U. S. A.*, 2004, **101**, 17988–17993.
16 J. J. van Thor, *Chem. Soc. Rev.*, 2009, **38**, 2935–2950.
17 J. J. van Thor, T. Gensch, K. J. Hellingwerf and L. N. Johnson, *Nat. Struct. Biol.*, 2002, **9**, 37–41.
18 T. M. H. Creemers, A. J. Lock, V. Subramaniam, T. M. Jovin and S. Völker, *Nat. Struct. Biol.*, 1999, **6**, 557–560.
19 S. R. Meech, *Chem. Soc. Rev.*, 2009, **38**, 2922–2934.
20 G.-J. Kremers, J. Goedhart, D. J. van den Heuvel, H. C. Gerritsen and T. W. J. Gadella, *Biochemistry*, 2007, **46**, 3775–3783.
21 R. Berera, R. van Grondelle and J. T. M. Kennis, *Photosynth. Res.*, 2009, **101**, 105–118.
22 I. H. M. van Stokkum, D. S. Larsen and R. van Grondelle, *Biochim. Biophys. Acta*, 2004, **1657**, 82–104.
23 G. J. Kremers, J. Goedhart, E. B. van Munster and T. W. J. Gadella, *Biochemistry*, 2006, **45**, 6570–6580.
24 G. J. Kremers, E. B. van Munster, J. Goedhart and T. W. J. Gadella, *Biophys. J.*, 2008, **95**, 378–389.
25 B. R. Rankin, G. Moneron, C. A. Wurm, J. C. Nelson, A. Walter, D. Schwarzer, J. Schroeder, D. A. Colón-Ramos and S. W. Hell, *Biophys. J.*, 2011, **100**, L63–L65.
26 G.-J. Zhao and K.-L. Han, *Acc. Chem. Res.*, 2012, **45**, 404–413.
27 S. W. Hell and J. Wichmann, *Opt. Lett.*, 1994, **19**, 780–782.
28 S. W. Hell, *Nat. Methods*, 2009, **6**, 24–32.
29 U. V. Nägerl, K. I. Willig, B. Hein, S. W. Hell and T. Bonhoeffer, *Proc. Natl. Acad. Sci. U. S. A.*, 2008, **105**, 18982–18987.
30 K. I. Willig, R. R. Kellner, R. Medda, B. Hein, S. Jakobs and S. W. Hell, *Nat. Methods*, 2006, **3**, 721–723.
31 B. Hein, K. I. Willig and S. W. Hell, *Proc. Natl. Acad. Sci. U. S. A.*, 2008, **105**, 14271–14276.
32 J.-i. Hotta, E. Fron, P. Dedecker, K. P. F. Janssen, C. Li, K. Müllen, B. Harke, J. Bückers, S. W. Hell and J. Hofkens, *J. Am. Chem. Soc.*, 2010, **132**, 5021–5023.
33 R. Kasper, B. Harke, C. Forthmann, P. Tinnefeld, S. W. Hell and M. Sauer, *Small*, 2010, **6**, 1379–1384.